

Efficient Robot Design with Multi-Objective Black-Box Optimization and Large Language Models

Kento Kawaharazuka¹, Yoshiki Obinata¹, Naoaki Kanazawa¹, Haoyu Jia¹, and Kei Okada¹

Abstract—Various methods for robot design optimization have been developed so far. These methods are diverse, ranging from numerical optimization to black-box optimization. While numerical optimization is fast, it is not suitable for cases involving complex structures or discrete values, leading to frequent use of black-box optimization instead. However, black-box optimization suffers from low sampling efficiency and takes considerable sampling iterations to obtain good solutions. In this study, we propose a method to enhance the efficiency of robot body design based on black-box optimization by utilizing large language models (LLMs). In parallel with the sampling process based on black-box optimization, sampling is performed using LLMs, which are provided with problem settings and extensive feedback. We demonstrate that this method enables more efficient exploration of design solutions and discuss its characteristics and limitations.

I. INTRODUCTION

The diversity of robot designs has been increasing, and their body structures, particularly joint configurations, differ significantly between robots. There are also an increasing number of modular robots that can change their bodies according to tasks or user preferences [1], [2].

As various robot configurations are being constructed, many studies have been developed to identify favorable configurations and optimize the design of body structures. For example, in [3], the number and types of modules, as well as their relative positions, have been optimized using a genetic algorithm to satisfy the target operation points for industrial robots. In [4], a multi-objective optimization of motor specifications and gear ratios for a general 6-DOF manipulator has been performed using a genetic algorithm to minimize body weight and maximize manipulability. In [5], the joint configuration and link lengths of a modular robot capable of traversing uneven terrain have been optimized using a graph heuristic search. In [6] an exhaustive search has been configured to design a modular robot that can execute tasks while satisfying joint angle limits, torque constraints, and collision avoidance. In [7], the design of a modular robot has been optimized by generating diverse body structures using a Generative Adversarial Network (GAN). In [8], evolutionary strategies have been employed to optimize the module configuration to satisfy the commanded trajectory while minimizing manipulability and required torque. The work in [9] has presented Pareto-optimal solutions that minimize position error and required torque through multi-objective optimization using a genetic algorithm for body

¹ The authors are with the Department of Mechano-Informatics, Graduate School of Information Science and Technology, The University of Tokyo, 7-3-1 Hongo, Bunkyo-ku, Tokyo, 113-8656, Japan. [kawaharazuka, obinata, kanazawa, jia, k-okada]@jsk.imi.i.u-tokyo.ac.jp

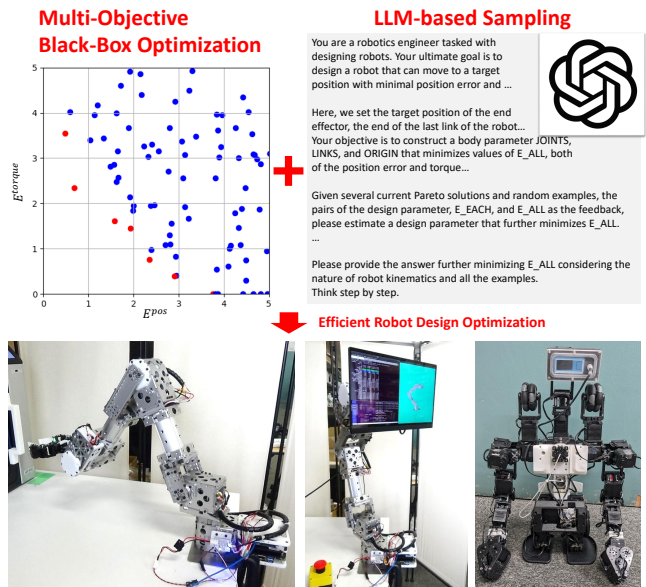


Fig. 1. The concept of this study: high efficiency robot design with multi-objective black-box optimization and LLM-based sampling.

adaptation to tasks and user preferences. In [10], body design optimization has been extended to include not only rotary joints but also linear joints.

As illustrated, various methods such as genetic algorithms, evolutionary strategies, exhaustive search, heuristic search, and GANs have been utilized for optimizing the body design of diverse robots. Among these, research using black-box optimization, particularly genetic algorithms, is prevalent due to its applicability to complex problem settings, including optimizations involving both continuous and discrete variables as well as multi-objective optimization [3], [4], [9]–[11]. Although gradient-free black-box optimization is applicable to any problem, it has the drawback of requiring a substantial number of samples and time to generate high-quality solutions.

As an alternative approach, examples of using large language models (LLMs) [12]–[14] for body design have begun to emerge. In [15], it is qualitatively demonstrated that LLMs can effectively assist in robot design. In [16], optimization of truss structures has been performed by leveraging LLMs and feedback from results. In [17], a modular robot design optimization has been conducted based on sequential prompt adjustments using an LLM. A notable feature of LLMs is their ability to output appropriate designs based on language instructions when provided with problem settings, context, and various examples. However, while LLMs are effective

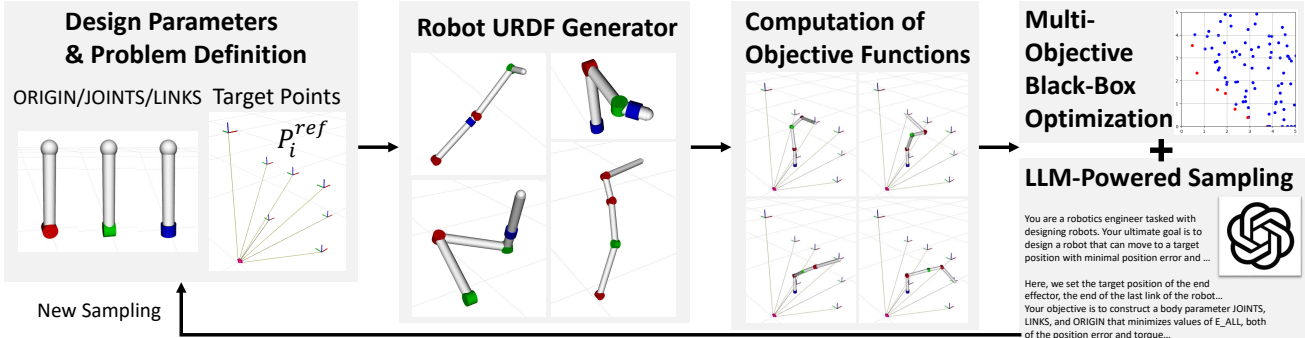


Fig. 2. The overview of the proposed robot design optimization. We set the robot design parameters, automatically generate the robot URDF, compute the objective functions, and perform multi-objective black-box optimization and LLM-based sampling.

for assisting with general design, they face challenges in fine-tuning detailed parameters.

To address this, we propose a method that combines black-box optimization with LLMs to enable more efficient output of design solutions. Our approach leverages the strength of black-box optimization for precise numerical adjustments and the capability of LLMs to produce broad design outputs. In parallel with the sampling process in conventional black-box optimization, sampling is also performed using an LLM, which is provided with prior knowledge, problem settings, and design examples. It should be noted that while the combination of LLMs and BBO has been shown to be effective for single-objective and general numerical problems [18], this study extends the approach to the more complex domain of multi-objective optimization in robot design. In this study, a multi-objective design optimization is conducted by adjusting the robot's base position, joint configuration, and link lengths to minimize the end-effector position error and the required torque for given operation points. We demonstrate that our method enables more efficient exploration of design solutions compared to black-box optimization alone, while also discussing the method's interesting characteristics and limitations.

The structure of this study is as follows. In Section II, we describe the problem setting, particularly the design parameters and objective functions. We also explain the sampling process using multi-objective black-box optimization and LLMs. In Section III, we present experimental results for three sets of target operation points. Several evaluation experiments are conducted, including examining changes in the results based on the proportion of LLM-based sampling and differences in prompts. Finally, we discuss the experimental results in Section IV and present our conclusions in Section V.

II. EFFICIENT ROBOT DESIGN WITH MULTI-OBJECTIVE BLACK-BOX OPTIMIZATION AND LLM-BASED SAMPLING

The problem setting of this study is briefly described (Fig. 2). Here, we focus on a robot arm with multiple joints connected in series. The robot is given target operation points P_i^{ref} ($1 \leq i \leq N_{ref}$, where N_{ref} is the number of target operation points). The objective of this study is to find Pareto-

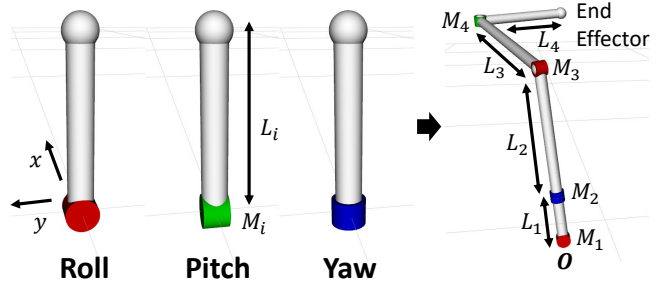


Fig. 3. The robot design parameters handled in this study. The parameters include the base link coordinate O , the joint types M , and the link lengths L of the robot.

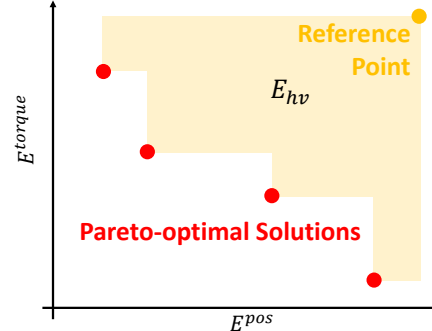


Fig. 4. Hypervolume for the evaluation of multi-objective optimization.

optimal solutions that minimize both the position error E^{pos} , which measures how accurately the robot reaches the target points, and the total joint torque E^{torque} required during the process. To achieve this objective, we utilize a combination of multi-objective black-box optimization (BBO) and large language models (LLMs).

In Section II-A, we describe the design parameters of the robot used in this study. In Section II-B, we explain the objective functions to be optimized. In Section II-C, we provide details on the sampling process using multi-objective black-box optimization. In Section II-D, we describe the sampling process that leverages LLMs.

A. Robot Design Parameters

The design parameters of the robot used in this study are shown in Fig. 3. The robot consists of D joints, and each joint M_j ($1 \leq j \leq D$) is configured as either a Roll, Pitch, or Yaw joint. Each joint is followed by a link of length L_j . In

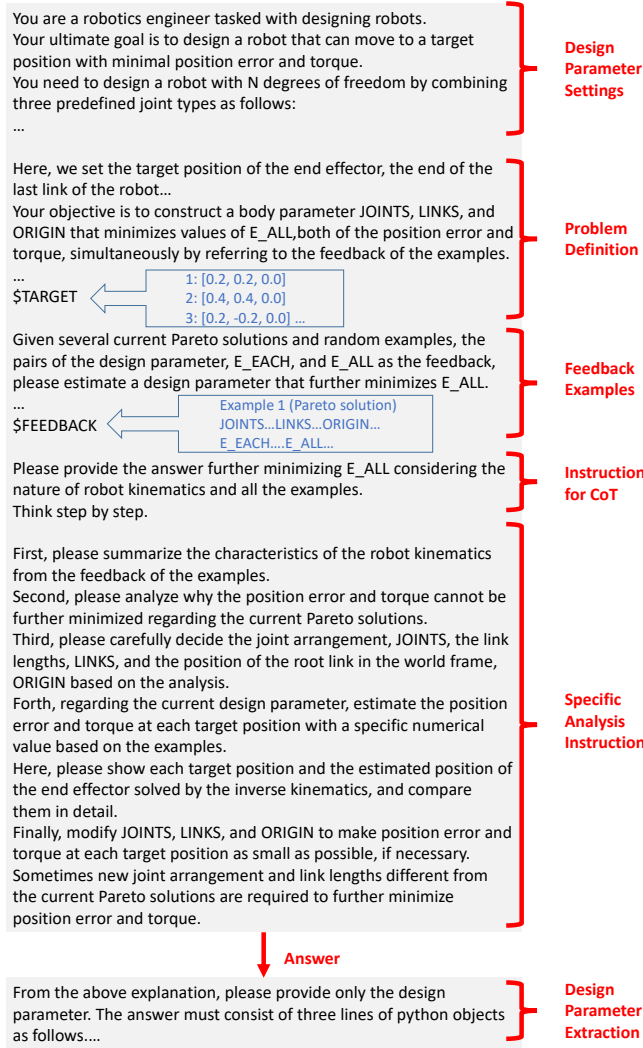


Fig. 5. The overview of the prompt for LLM-based sampling conducted in this study.

this study, each joint can move within the range of $[-2.4, 2.4]$ rad, and the length of each link is set within the range of $[0.03, 0.3]$ m. When all joint angles are set to 0, all links align vertically in a straight line. Additionally, the base link coordinate \mathbf{O} of the robot in 3D space is also treated as a design parameter. This assumes that the robot is properly positioned for the task, particularly in systems such as mobile robots. The first joint M_1 of the robot is placed at coordinate \mathbf{O} . The values of \mathbf{O} in the x , y , and z directions are within the range $-1.0 \leq O_{x,y,z} \leq 1.0$ m. Thus, the full set of design parameters for the robot consists of \mathbf{O} , \mathbf{M} , and \mathbf{L} , forming a $2D + 3$ dimensional vector that includes both discrete and continuous values. Once these parameters are determined, the corresponding Unified Robot Description Format (URDF) of the robot can be automatically generated.

B. Objective Functions

The objective functions for robot design optimization can take various forms; however, in this study, we use a relatively simple formulation consisting of the position error E^{pos} with respect to the target positions and the joint torque E^{torque} .

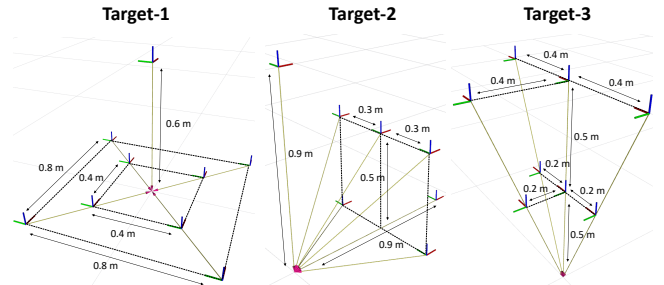


Fig. 6. Experimental setup of the three target operation points: Target-1, Target-2, and Target-3.

These functions are defined as follows.

$$E^{\text{pos}} = \sum_i^{N_{\text{ref}}} \|\mathbf{P}_i^{\text{ik}} - \mathbf{P}_i^{\text{ref}}\|_2 \quad (1)$$

$$E^{\text{torque}} = \alpha \sum_i^{N_{\text{ref}}} \|\boldsymbol{\tau}_i^{\text{ik}}\|_2 \quad (2)$$

where \mathbf{P}_i^{ik} and $\boldsymbol{\tau}_i^{\text{ik}}$ represent the end-effector position and gravity-compensation torque, respectively, when the robot solves the inverse kinematics (IK) to reach the target position $\mathbf{P}_i^{\text{ref}}$, assuming the robot's initial posture has all joint angles set to zero. The inverse kinematics algorithm used in this study is based on the methods described in [19], [20]. In other words, this evaluates whether the target end-effector position can be achieved with that body design, and how much joint torque is required in doing so. Of course, it is also possible to consider not only the target position but also the orientation, or to use a more complex evaluation function.

Note that, for simplicity, the posture of the target points is ignored, and only the reachability to the target positions is considered. Additionally, the coefficient α (set to $\alpha = 40$ in this study) is multiplied by E^{torque} to scale it to a similar magnitude as E^{pos} for clarity.

C. Multi-Objective Black-Box Optimization

In this study, we address a multi-objective optimization problem that aims to minimize both objective functions E^{pos} and E^{torque} . This allows us to obtain various design solutions from the Pareto-optimal set. For the multi-objective optimization, we use the Tree-Structured Parzen Estimator (TPE) [21] implemented in the black-box optimization library Optuna [22]. TPE supports multi-objective optimization and is notable for requiring a relatively small recommended sample size of fewer than 1000. Although NSGA-II [23] is also commonly used, this study adopted TPE, which can obtain good solutions with fewer samples.

To evaluate the performance of the multi-objective optimization, we use Hypervolume [24] as a metric to measure how effectively good design solutions are explored. As shown in Fig. 4, the hypervolume E_{hv} is defined as the area enclosed by the Pareto-optimal solutions (represented by red points) and the reference point. A larger hypervolume indicates that more favorable design solutions have been explored. In this study, the reference point is set to $(5.0, 5.0)$.

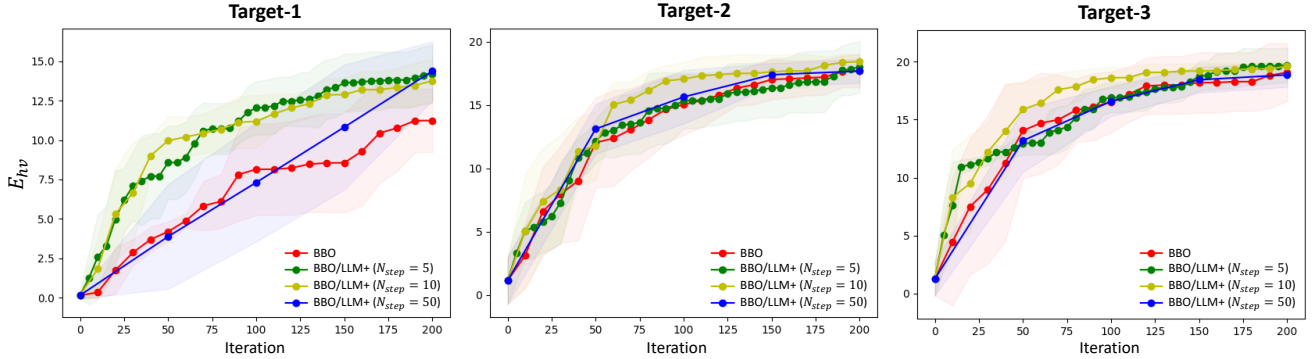


Fig. 7. Comparison of **BBO**, **BBO/LLM+** ($N_{step} = 5$), **BBO/LLM+** ($N_{step} = 10$), and **BBO/LLM+** ($N_{step} = 50$) for Target-1, Target-2, and Target-3.

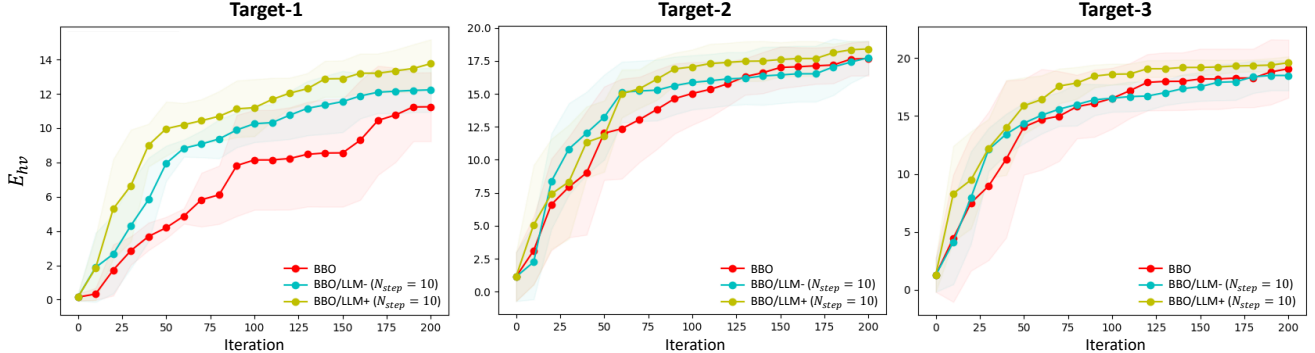


Fig. 8. Comparison of **BBO**, **BBO/LLM-** ($N_{step} = 10$), and **BBO/LLM+** ($N_{step} = 10$) for Target-1, Target-2, and Target-3.

D. LLM-based Design Sampling

In parallel with the multi-objective optimization sampling described above, sampling using a large language model is also performed. The LLM utilizes In-context Learning [25] to output the next design parameters to explore based on the given problem setting and feedback from previously obtained solutions. The actual prompt, feedback on the solutions, and the subsequent output formatting steps are illustrated in Fig. 5.

First, as shown at the top of Fig. 5, the design parameters and problem setting of this study are described, and the target position \mathbf{P}_i^{ref} is input into \$TARGET. Next, as feedback, N_{pareto} solutions are randomly selected from the Pareto-optimal solutions and N_{random} solutions are selected from the overall sampling results. The information for each solution includes the ORIGIN \mathbf{O} , JOINTS \mathbf{M} , and LINKS \mathbf{L} , the evaluation values E_EACH (E_i^{pos}, E_i^{torque}) for each \mathbf{P}_i^{ref} , the end-effector positions \mathbf{P}_i^{ik} and the joint torques τ_i^{ik} obtained from the inverse kinematics solution, and the overall evaluation values E_ALL (E^{pos}, E^{torque}). Instructions for Chain-of-Thought (CoT) reasoning, such as “Think step by step” [26], and additional instructions on how to analyze specific parameters are provided. When only general CoT instructions are given, we refer to the approach as **LLM**, while the approach that includes specific parameter analysis instructions tailored to this study is referred to as **LLM+**. The output obtained from this process is reformatted by the LLM to provide design parameters in the form of a Python List or Tuple. The generated solutions are then added to the sampling process of the multi-objective optimization.

The optimization process starts with N_{init} random sampling steps. After that, the optimization proceeds in steps of N_{step} , where one sampling step is performed using the LLM, followed by $N_{step} - 1$ sampling steps using multi-objective black-box optimization. Although these processes can be executed in parallel, this sequential approach is adopted for ease of evaluation. The smaller the N_{step} is, the greater the influence of the LLM is. By varying N_{step} , it is possible to evaluate the degree to which the LLM contributes to the optimization. Although N_{init} is typically included in the total optimization attempts, for clarity, we reset the count to 0 after the N_{init} random trials and perform a total of N_{total} sampling steps.

III. EXPERIMENTS

A. Experimental Setup

In this study, experiments are conducted for three sets of target operation points, Target-1, Target-2, and Target-3, as shown in Fig. 6. For each target operation point, we compare **BBO**, which uses only black-box optimization, and **BBO/LLM+**, which combines black-box optimization with a large language model. To evaluate the extent of LLM’s contribution to the optimization process, we vary N_{step} , which represents the number of black-box optimization steps performed between each LLM-based sampling. In this study, experiments are conducted with $N_{step} = 5, 10, 50$. Additionally, we perform a comparative evaluation of **BBO/LLM-**, which uses general Chain-of-Thought reasoning without specific parameter analysis instructions. The other parameters are set as follows: $D = 4$, $N_{init} = 10$, $N_{pareto} = 5$,

$N_{random} = 5$, and $N_{total} = 200$. Each experiment is repeated five times with different random seed values, and the mean and standard deviation of the results are reported.

TABLE I

COMPARISON OF HYPERVOLUME E_{hv} AND ITS STANDARD DEVIATION σ_{hv} FOR BBO, BBO/LLM-, AND BBO/LLM+

Method	Target-1		Target-2		Target-3	
	$E_{hv} \uparrow$	$\sigma_{hv} \downarrow$	$E_{hv} \uparrow$	$\sigma_{hv} \downarrow$	$E_{hv} \uparrow$	$\sigma_{hv} \downarrow$
BBO	6.70	2.03	13.16	2.39	14.64	3.43
BBO/LLM-	8.85	1.38	13.87	2.33	14.73	1.67
BBO/LLM+	10.25	1.42	14.43	1.89	16.29	1.53

B. Experimental Results

The experimental results are presented below. Fig. 7 shows a comparison of the methods **BBO**, **BBO/LLM+** ($N_{step} = 5$), **BBO/LLM+** ($N_{step} = 10$), and **BBO/LLM+** ($N_{step} = 50$) for Target-1, Target-2, and Target-3. The horizontal axis represents the optimization iterations, and the vertical axis represents the hypervolume E_{hv} . The figure illustrates how E_{hv} changes with different values of N_{step} . A general trend observed is that **BBO/LLM+** ($N_{step} = 10$) consistently demonstrates the best results across all target operation points, confirming the effectiveness of LLM-based sampling. For Target-1, the improvement is particularly significant, while for Target-2 and Target-3, the impact is less pronounced, indicating that the effectiveness of LLM sampling depends on the target operation points. For $N_{step} = 50$, only four LLM-based samplings occur within 200 sampling steps, making the trend of E_{hv} similar to that of **BBO**. For $N_{step} = 5$, although LLM-based sampling occurs more frequently and is effective in the early stages for Target-1 and Target-2, the results are inferior compared to $N_{step} = 10$.

Fig. 8 shows a comparison of **BBO**, **BBO/LLM-** ($N_{step} = 10$), and **BBO/LLM+** ($N_{step} = 10$). The general trend indicates that **BBO/LLM-** performs better than **BBO**, but it is inferior to **BBO/LLM+**, demonstrating the importance of adding specific parameter analysis instructions. The average hypervolume E_{hv} over all iterations and the average standard deviation σ_{hv} of E_{hv} are shown in Table I. The numerical results confirm the performance trend of **BBO** < **BBO/LLM-** < **BBO/LLM+**. Moreover, the values of σ_{hv} for **BBO/LLM-** and **BBO/LLM+** are smaller than those for **BBO**, indicating that LLM-based sampling reduces randomness and leads to more stable results.

C. Target-1 Experiment

We now discuss the experimental results for each target operation point, focusing on **BBO/LLM+** ($N_{step} = 10$). First, we explain how to interpret the figures using Fig. 9 as an example. The top section of the figure shows the sampling results after 10, 70, 130, and 200 iterations, where each point represents a sampling result obtained from either BBO or LLM. The horizontal axis represents E^{pos} , and the vertical axis represents E^{torque} , with Pareto-optimal solutions displayed in a different color. Two Pareto-optimal

solutions, Solution 1 and Solution 2, are selected from the results after 200 iterations, and the designs and inverse kinematics results for each target operation point are shown in the bottom section of the figure.

We describe the experimental results for Target-1 (Fig. 9). In the case of Target-1, many of the Pareto-optimal solutions across iterations are obtained from LLM-based sampling. Solution 1 represents a solution with low E^{pos} but high E^{torque} , while Solution 2 is the opposite, featuring low E^{torque} but higher E^{pos} .

Solution 1 places \mathbf{O} at the origin in 3D space, providing easy access to all target operation points, and adopts a joint arrangement of $Y - P - R - P$ (where R represents Roll, P represents Pitch, and Y represents Yaw), achieving uniform reachability across all operation points. In contrast, Solution 2 shifts \mathbf{O} in the negative z -axis direction and adopts a joint arrangement of $Y - Y - P - Y$, which reduces reachability to the target operation points but minimizes the required torque.

As an example, Fig. 10 shows a portion of the LLM output when Solution 1 was sampled. In Step 1, the characteristics of each parameter are analyzed. In Step 2, the current issues with the Pareto-optimal solutions are examined. In Step 3, the LLM outputs the new set of design parameters. In the analysis of the joint arrangement in Step 2, many of the previous solutions used multiple joints of the same type consecutively, but the LLM explicitly changed this to the arrangement $Y - P - R - P$. Additionally, in Step 3, the base link coordinate \mathbf{O} is set precisely at the origin to secure a symmetric workspace. The ability to secure a symmetric workspace is particularly important for Target-1, as placing \mathbf{O} at the origin significantly simplifies the problem. This type of reasoning is difficult for black-box optimization alone. However, the LLM can determine an appropriate \mathbf{O} based on the problem setting, demonstrating the effectiveness of LLM-based sampling in achieving better design solutions.

D. Target-2 Experiment

We describe the experimental results for Target-2 (Fig. 11). In the case of Target-2, LLM-based sampling also accounts for many of the Pareto-optimal solutions, confirming its effectiveness. Unlike Target-1, the joint structure for both Solution 1 and Solution 2 is the same, $Y - R - P - R$. However, the second and fourth links in Solution 1 are longer compared to those in Solution 2. Due to this difference, Solution 1 achieves a lower E^{pos} , while Solution 2 achieves a lower E^{torque} . In Solution 2, the lengths of the first and second links are set to approximately 0.5 m, allowing the second link to match the height of the target operation points. The remaining joints are then used in a manner similar to a SCARA-type structure, helping to minimize the required torque.

E. Target-3 Experiment

We describe the experimental results for Target-3 (Fig. 12). For Target-3, while LLM-based sampling contributes to the results, the effect of BBO-based sampling is more prominent. Solution 1 adopts a joint arrangement of $Y - P - P - Y$

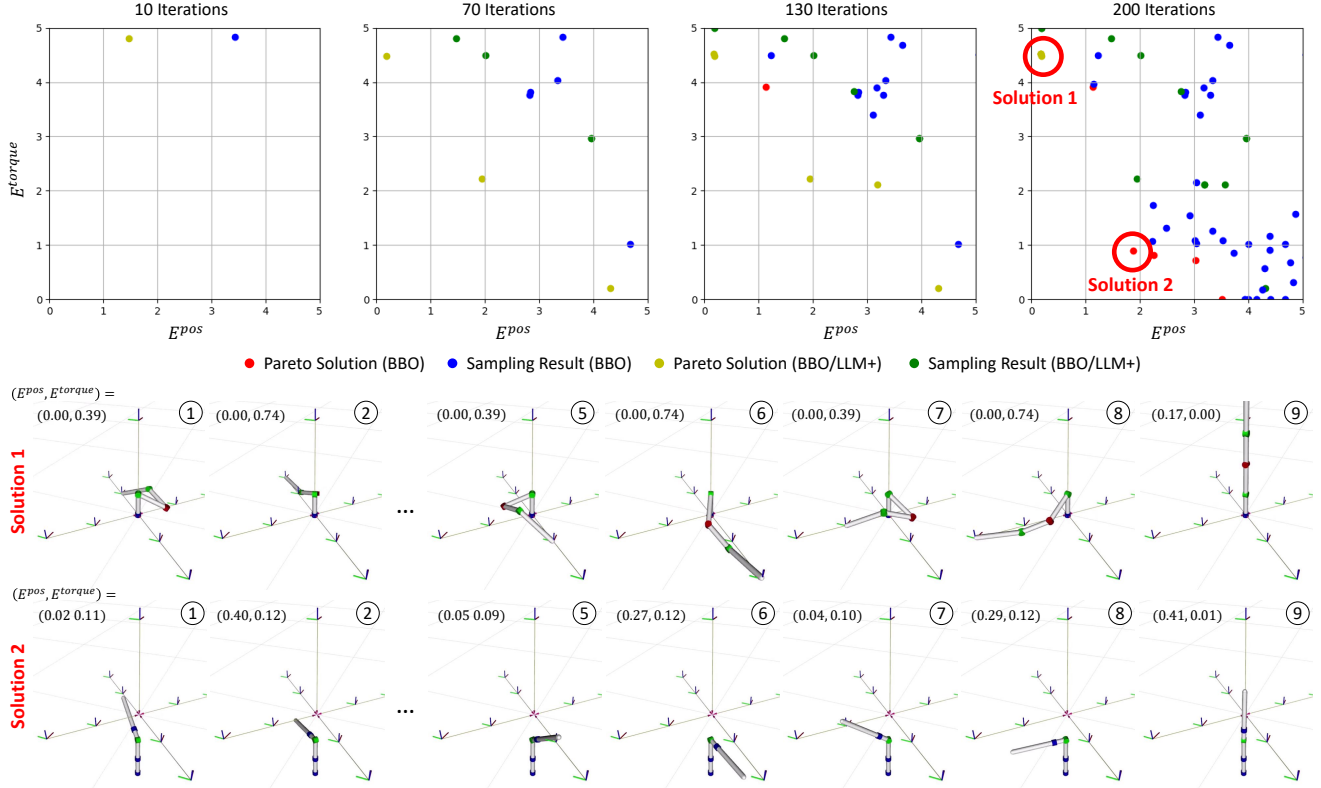


Fig. 9. The sampling results of Target-1 for BBO/LLM+ ($N_{\text{step}} = 10$) and the selected Pareto-optimal solutions.

and places \mathbf{O} near the center of all target operation points, thereby minimizing E_{pos} . In contrast, Solution 2 uses a joint arrangement of $Y - Y - P - Y$, reducing the number of pitch axes that are prone to high torque, and shifts \mathbf{O} further in the negative z -axis direction to minimize E_{torque} . The approach to constructing the solutions is similar to that of Target-1.

IV. DISCUSSION

We discuss the experimental results obtained in this study. First, we summarize the overall trends. LLM-based sampling was effective across multiple problems, although the degree of effectiveness varied for each. Additionally, the performance was found to be influenced by the ratio of LLM-based sampling to BBO-based sampling. Furthermore, the performance of LLM-based sampling varied significantly depending on the prompt configuration. In particular, by incorporating the specific parameter analysis instructions proposed in this study, better design solutions could be explored. It was also observed that LLM-based sampling enabled solutions that are difficult for black-box optimization alone, such as placing \mathbf{O} precisely at the origin or ensuring a symmetric workspace along the xz -plane. Additionally, it was confirmed that LLM-based sampling reduced randomness and produced more stable results. However, it was also noted that values such as link lengths tended to be output as rounded values, making it difficult to perform fine-tuned adjustments.

Next, we consider the execution time of LLM-based sampling. Although LLM inference has gradually become faster, each inference still takes approximately 1-2 seconds.

However, this issue becomes negligible if LLM-based sampling is executed fully in parallel with BBO. In many cases, performance improvements were observed when LLM-based sampling was performed even once for every nine BBO sampling steps. This suggests that running LLM-based sampling in parallel, without much consideration, could potentially lead to more efficient sampling.

Finally, we discuss the limitation of the proposed method. In this study, we adopted a relatively straightforward and general problem setting. However, in real-world robot design, it is often necessary to consider more complex constraints, joint structures, and link geometries. The extent to which LLMs can contribute to design optimization depends on their spatial reasoning capabilities and the complexity of the problem setting. While this study primarily focused on demonstrating a new concept, future work will aim to develop a system that can be applied to more complex problem settings.

V. CONCLUSION

In this study, we proposed a robot design optimization method that leverages LLM-based sampling alongside black-box optimization. By providing broad design guidelines through LLMs, it is possible to output solutions more efficiently than before, thereby improving the sampling efficiency of black-box optimization. LLM-based sampling needs to be used in an appropriate ratio alongside black-box optimization, and the configuration of the LLM prompt has a significant impact on the results. In particular, adding specific parameter analysis instructions enables the exploration of

Step 1: Summarize the Characteristics of the Robot Kinematics

- Joint Types and Arrangements:** The examples show a variety of joint arrangements, primarily using combinations of 'Y', 'P', and 'R' joints. The choice of joint types affects the robot's ability to reach certain positions and orientations.
- Link Lengths:** The link lengths vary between 0.03 and 0.30 meters. The distribution of these lengths affects the reach and flexibility of the robot.
- Origin Position:** The position of the root link in the world frame influences the initial configuration and workspace of the robot.

...

Step 2: Analyze Why Position Error and Torque Cannot Be Further Minimized

- Joint Arrangement:** The current Pareto solutions use specific joint arrangements that may not be optimal for all target positions. For instance, using too many of the same joint type can limit the robot's ability to reach certain positions efficiently.
- Link Lengths:** The link lengths in the Pareto solutions may not be ideal for all target positions, leading to higher position errors or torque.
- Origin Position:** The origin position might not be optimal for minimizing the position error and torque across all target positions.

Step 3: Decide on JOINTS, LINKS, and ORIGIN

- JOINTS:** A balanced combination of 'Y', 'P', and 'R' joints can provide better flexibility and reach. Consider using a 'Y', 'P', 'R', 'P' arrangement to allow for diverse movement capabilities.
- LINKS:** Choose link lengths that provide a good balance between reach and precision. For example, [0.1, 0.2, 0.15, 0.25] could be a good starting point, as seen in some Pareto solutions.
- ORIGIN:** Set the origin to a neutral position, such as (0.0, 0.0, 0.0), to provide a symmetric workspace.

...

Fig. 10. An overview of LLM output for Solution 1 in Target-1 experiment.

better design solutions. This approach makes it possible to explore symmetric design solutions, which are challenging for black-box optimization alone, and it has been shown to be highly effective depending on the problem setting. In the future, we aim to develop a system that can quickly propose personalized robot body designs based on user tasks and preferences.

REFERENCES

- R. J. Alattas, S. Patel, and T. M. Sobh, "Evolutionary Modular Robotics: Survey and Analysis," *Journal of Intelligent & Robotic Systems*, vol. 95, no. 3, pp. 815–828, 2019.
- E. Romiti, J. Malzahn, N. Kashiri, F. Iacobelli, M. Ruzzon, A. Laurenzi, E. M. Hoffman, L. Muratore, A. Margan, L. Baccelliere, S. Cordasco, and N. Tsagarakis, "Toward a Plug-and-Work Reconfigurable Cobot," *IEEE/ASME Transactions on Mechatronics*, vol. 27, no. 5, pp. 3219–3231, 2022.
- G. Yang and I. Chen, "Task-based optimization of modular robot configurations: minimized degree-of-freedom approach," *Mechanism and Machine Theory*, vol. 35, no. 4, pp. 517–540, 2000.
- Y. Xiao, Z. Fan, W. Li, S. Chen, L. Zhao, and H. Xie, "A Manipulator Design Optimization Based on Constrained Multi-objective Evolutionary Algorithms," in *2016 International Conference on Industrial Informatics*, 2016, pp. 199–205.
- A. Zhao, J. Xu, M. K. Luković, J. Hughes, A. Speilberg, D. Rus, and W. Matusik, "RoboGrammar: Graph Grammar for Terrain-Optimized Robot Design," *ACM Transactions on Graphics*, vol. 39, no. 6, pp. 1–16, 2020.
- S. B. Liu and M. Althoff, "Optimizing performance in automation through modular robots," in *2020 IEEE International Conference on Robotics and Automation*, 2020, pp. 4044–4050.
- M. Lei, E. Romiti, A. Laurenzi, and N. G. Tsagarakis, "Task-Driven Computational Framework for Simultaneously Optimizing Design and Mounted Pose of Modular Reconfigurable Manipulators," in *2024 IEEE/RSJ International Conference on Intelligent Robots and Systems*, 2024.
- J. Hu, J. Whitman, M. Travers, and H. Choset, "Modular Robot Design Optimization with Generative Adversarial Networks," in *2022 IEEE International Conference on Robotics and Automation*, 2022, pp. 4282–4288.
- K. Kawaharazuka, T. Makabe, K. Okada, and M. Inaba, "Daily Assistive Modular Robot Design Based on Multi-Objective Black-Box Optimization," in *2023 IEEE/RSJ International Conference on Intelligent Robots and Systems*, 2023, pp. 9970–9977.
- K. Kawaharazuka, K. Okada, and M. Inaba, "Robot Design Optimization with Rotational and Prismatic Joints Using Black-Box Multi-Objective Optimization," in *2024 IEEE/RSJ International Conference on Intelligent Robots and Systems*, 2024, pp. 4571–4577.
- P. R. Vanteddu, G. Nava, F. Bergonti, G. L'Erario, A. Paolino, and D. Pucci, "From CAD to URDF: Co-Design of a Jet-Powered Humanoid Robot Including CAD Geometry," in *2024 IEEE/RSJ International Conference on Intelligent Robots and Systems*, 2024.
- T. B. Brown, B. Mann, N. Ryder, M. Subbiah, J. Kaplan, P. Dhariwal, A. Neelakantan, P. Shyam, G. Sastry, A. Askell, S. Agarwal, A. Herbert-Voss, G. Krueger, T. Henighan, R. Child, A. Ramesh, D. M. Ziegler, J. Wu, C. Winter, C. Hesse, M. Chen, E. Sigler, M. Litwin, S. Gray, B. Chess, J. Clark, C. Berner, S. McCandlish, A. Radford, I. Sutskever, and D. Amodei, "Language Models are Few-Shot Learners," in *2020 Neural Information Processing Systems*, 2020, pp. 1877–1901.
- J. Achiam, S. Adler, S. Agarwal, L. Ahmad, I. Akkaya, F. L. Aleman, D. Almeida, J. Alten Schmidt, S. Altman, S. Anadkat *et al.*, "Gpt-4 technical report," *arXiv preprint arXiv:2303.08774*, 2023.
- K. Kawaharazuka, T. Matsushima, A. Gambardella, J. Guo, C. Paxton, and A. Zeng, "Real-World Robot Applications of Foundation Models: A Review," *Advanced Robotics*, vol. 38, no. 18, pp. 1232–1254, 2024.
- F. Stella, C. D. Santina, and J. Hughes, "How can LLMs transform the robotic design process?" *Nature machine intelligence*, vol. 5, no. 6, pp. 561–564, 2023.
- Y. Jadhav and A. B. Farimani, "Large Language Model Agent as a Mechanical Designer," *arXiv preprint arXiv:2404.17525*, 2024.
- K. Qiu, K. Ciebiera, P. Fijałkowski, M. Cygan, and L. Kuciński, "RoboMorph: Evolving Robot Morphology using Large Language Models," *arXiv preprint arXiv:2407.08626*, 2024.
- T. Liu, N. Astorga, N. Seedat, and M. van der Schaar, "Large language models to enhance bayesian optimization," *arXiv preprint arXiv:2402.03921*, 2024.
- T. F. Chan and R. V. Dubey, "A weighted least-norm solution based scheme for avoiding joint limits for redundant joint manipulators," *IEEE Transactions on Robotics and Automation*, vol. 11, no. 2, pp. 286–292, 1995.
- H. Sugiura, M. Gienger, H. Janssen, and C. Goerick, "Real-time collision avoidance with whole body motion control for humanoid robots," in *2007 IEEE/RSJ International Conference on Intelligent Robots and Systems*, 2007, pp. 2053–2058.
- J. S. Bergstra, R. Bardenet, Y. Bengio, and B. Kégl, "Algorithms for Hyper-Parameter Optimization," in *2011 Neural Information Processing Systems*, 2011, pp. 2546–2554.
- T. Akiba, S. Sano, T. Yanase, T. Ohta, and M. Koyama, "Optuna: A Next-generation Hyperparameter Optimization Framework," in *25th ACM SIGKDD International Conference on Knowledge Discovery and Data Mining*, 2019.
- K. Deb, A. Pratap, S. Agarwal, and T. Meyarivan, "A fast and elitist multiobjective genetic algorithm: NSGA-II," *IEEE Transactions on Evolutionary Computation*, vol. 6, no. 2, pp. 182–197, 2002.
- E. Zitzler, "SPEA2: Improving the Strength Pareto Evolutionary Algorithm," 2001.
- Q. Dong, L. Li, D. Dai, C. Zheng, J. Ma, R. Li, H. Xia, J. Xu, Z. Wu, T. Liu *et al.*, "A survey on in-context learning," *arXiv preprint arXiv:2301.00234*, 2022.
- T. Kojima, S. S. Gu, M. Reid, Y. Matsuo, and Y. Iwasawa, "Large language models are zero-shot reasoners," *Advances in neural information processing systems*, vol. 35, pp. 22 199–22 213, 2022.

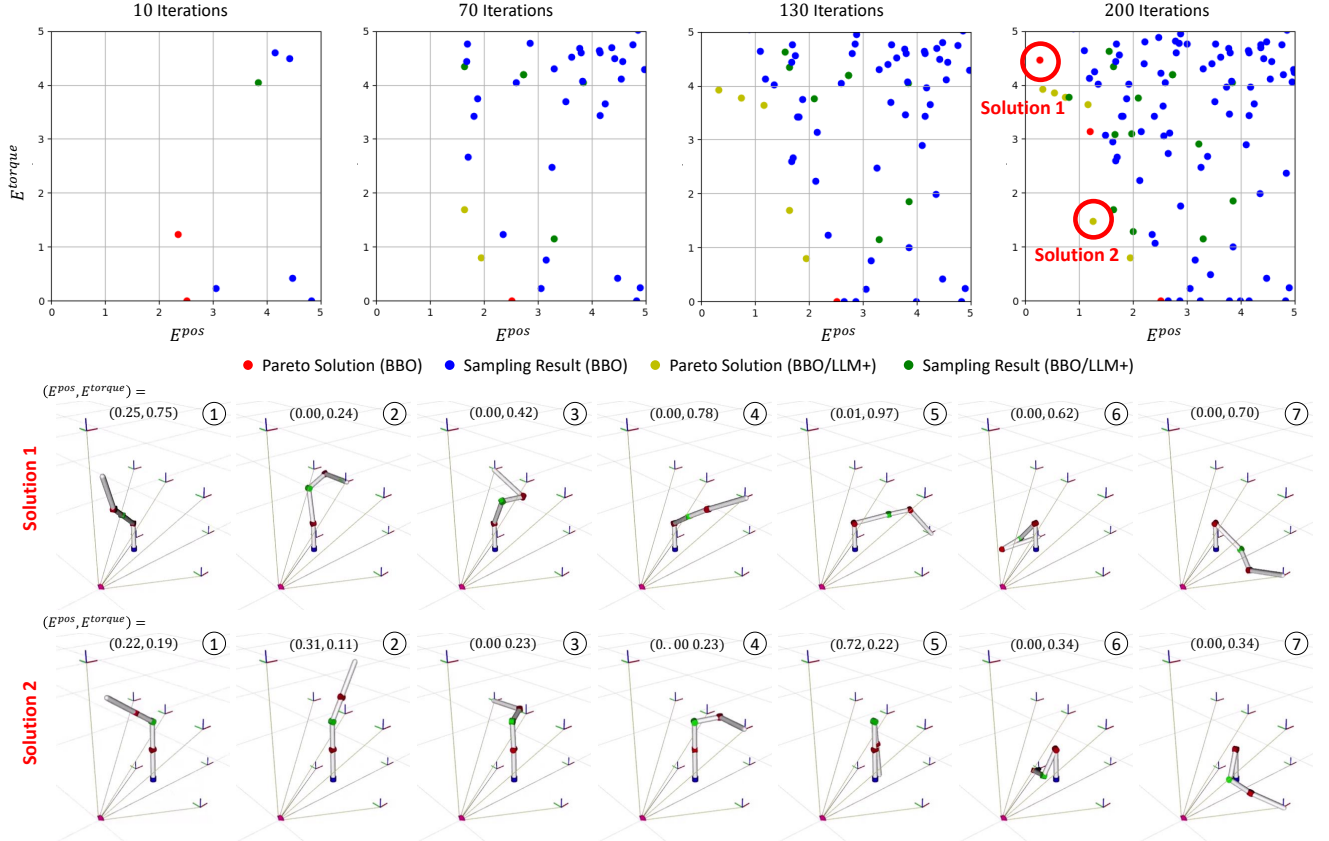


Fig. 11. The sampling results of Target-2 for BBO/LLM+ ($N_{step} = 10$) and the selected Pareto-optimal solutions.

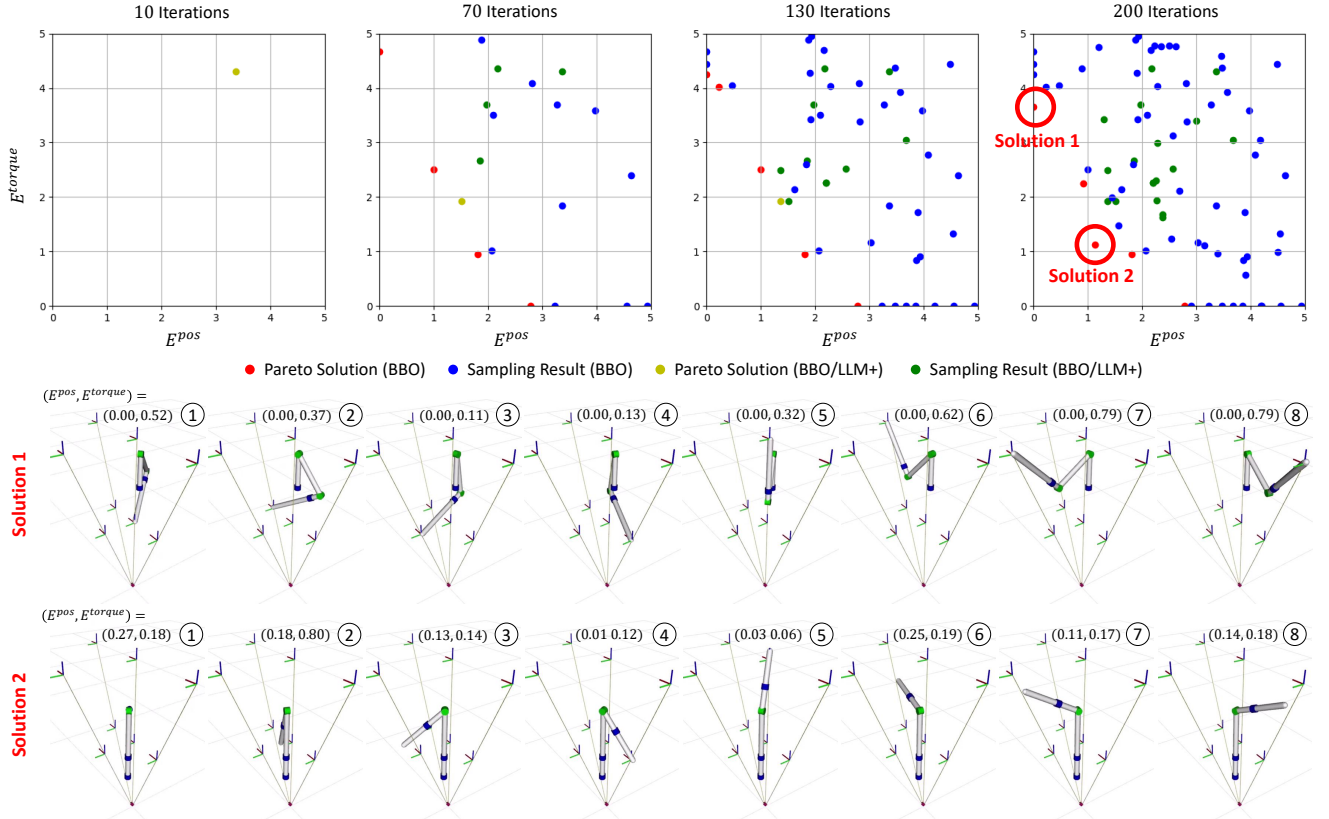


Fig. 12. The sampling results of Target-3 for BBO/LLM+ ($N_{step} = 10$) and the selected Pareto-optimal solutions.